Route to minimally dissipative switching in magnets via terahertz phonon pumping

STRUNGARU, Mara <http://orcid.org/0000-0003-4606-7131>, ELLIS, Matthew OA <http://orcid.org/0000-0003-0338-8920>, RUTA, Sergiu <http://orcid.org/0000-0001-8665-6817>, EVANS, Richard FL <http://orcid.org/0000-0002-2378-8203>, CHANTRELL, Roy W <http://orcid.org/0000-0001-5410-5615> and CHUBYKALO-FESENKO, Oksana <http://orcid.org/0000-0002-4081-1831>

Published version

STRUNGARU, Mara, ELLIS, Matthew OA, RUTA, Sergiu, EVANS, Richard FL, CHANTRELL, Roy W and CHUBYKALO-FESENKO, Oksana (2024). Route to minimally dissipative switching in magnets via terahertz phonon pumping. Physical Review B, 109 (22): 224412.

Route to minimally dissipative switching in magnets via terahertz phonon pumping

Mara Strungaru [1,*] Matthew O. A. Ellis [2] Sergiu Ruta [3] Richard F. L. Evans [1]
Roy W. Chantrell [1] and Oksana Chubykalo-Fesenko [4,†]

[1]*School of Physics, Engineering and Technology, University of York, York, YO10 5DD United Kingdom*
[2]*Department of Computer Science, University of Sheffield, Sheffield, S1 4DP, United Kingdom*
[3]*College of Business, Technology and Engineering, Sheffield Hallam University, Sheffield, S1 1WB, United Kingdom*
[4]*Instituto de Ciencia de Materiales de Madrid, CSIC, Cantoblanco, 28049 Madrid, Spain*

(Received 4 October 2022; revised 12 April 2024; accepted 14 May 2024; published 7 June 2024)

Ultrafast switching of magnetic materials has been shown to be predominantly thermally driven, but excess heating limits the energy efficiency of this process. By employing atomistic spin-lattice dynamics simulations, we show that efficient coherent magnetization switching of an insulating magnet can be triggered by a THz excitation of phonons. We find that switching is driven by excitation near the P point of the phonon spectrum in conditions where spins typically cannot be excited and when manifold k phonon modes are accessible at the same frequency. Our model determines the necessary ingredients for low-dissipative switching and provides insight into THz-excited spin dynamics with a route to energy efficient ultrafast devices.

DOI: 10.1103/PhysRevB.109.224412

I. INTRODUCTION

The control of magnetic order on an ultrafast timescale in an efficient and robust manner is crucial for the development of next-generation magnetic devices [1]. The interaction of magnetic materials with femtosecond laser pulses has shown multiple fundamental effects that culminate in the ability to switch the magnetization by means of purely optical excitation [2,3]. However, in metallic systems this is accompanied by a large rapid temperature increase, which is detrimental to the long-term usage of device. The use of insulators can be beneficial in this respect, however, the routes for energy efficient switching, involving minimal energy losses, still needs to be found.

A number of possibilities have been presented recently using ultrafast excitations in the terahertz (THz) regime by means of femtosecond lasers or THz sources [4]. One of the fundamental questions in this research is understanding the angular momentum transfer between spins and lattice, with recent results demonstrating that angular momentum transfer between both systems primarily takes place on an ultrashort timescale (around 200fs) [5], in contrast with previously considered timescales in the range of 100 ps [6]. Therefore, at the picosecond timescale and below, the dynamics of spin and lattice occurs simultaneously and one system can excite the other. First, excitation of the lattice can change magnetic parameters such as exchange [7–9] or anisotropy [10] and therefore can excite magnetization dynamics. Reciprocally, ultrafast excitation of the spin system can produce excitation of the lattice at the same timescale. An example of that is the ultrafast Einstein-de Haas effect [5] or localized spin-Peltier effect in antiferromagnets [11].

The most exciting results, however, are related to the possibility of magnetization switching via THz phonon pumping. Such a possibility was anticipated by theoretical investigations [12,13] based on a phenomenological model which includes magnetoelastic anisotropy. Recent experiments by Stupakiewicz *et al.* [14] demonstrated ultrafast magnetization switching in the magnetic insulator YIG by means of resonant pumping of specific longitudinal optical phonon modes. The switching was explained by excitations of local stresses that induce magnetoelastic anisotropy. The results also suggest a universal ultrafast switching mechanism which may be applied to a wide range of materials.

Thus, energy-efficient magnetization switching is particularly interesting to explore in insulators. This is due to the fact that, first, the electronic system with its low specific heat can have little participation in the energy uptake and, second, that excitation of the spin-phonon system on the subpicosecond timescale will have minimal interaction with the outside world in terms of energy diffusion. Therefore, one can try to find conditions for almost dissipationless ("cold") switching.

In this paper, we employ a spin-lattice framework as implemented in Ref. [15] able to treat both magnons and phonons in a self consistent way. Spin-lattice dynamics frameworks [6,16–21] have been used also to tackle other phenomena that involve magnon-phonon interaction such as the Einstein de-Haas effect that appears as a result of conservation of angular momentum [22,23]. Besides periodic systems, spin-lattice dynamics frameworks can also investigate finite-size systems such as magnetic nanoparticles [24,25] or ways

*mara.strungaru@york.ac.uk
†oksana@icmm.csic.es

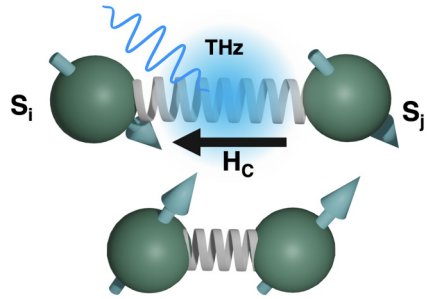

FIG. 1. Illustration of magnetization switching by THz pulses. The THz pulse couples directly to the lattice creating a magnetoelastic field that leads to low dissipation switching.

to parameterize more effectively the energy terms in such models [26], including first-principles parametrization [19,27] or machine-learning approaches [28].

Here we demonstrate the possibility of an energy-efficient switching in conditions when phonons are excited with high k values and THz frequencies, corresponding to a maximum in the density of states with no available spin-wave modes. A schematic representation of the process is provided in Fig. 1. The mechanism of switching is via local magnetoelastic fields created by atomic displacements due to the phonon pulse. The mK spin temperature developed during the switching process shows that the switching process can be considered nondissipative. Within dissipationless switching, one can think that the main mechanism behind it is angular momentum transfer between phonons to spins. Our findings indicate that the angular momentum pumped during excitation is not solely responsible for the observed switching. Instead, we demonstrate that switching is triggered by the presence of magnetoelastic fields. Furthermore, once the switching initiates, all generated angular momentum dissipates back into the lattice.

II. METHODOLOGY

The computational model for this paper has been previously employed in the systematic investigation of equilibrium and dynamic properties of of spins and phonons in BCC Fe [15]. However, the aim of this paper is not to model bcc Fe, the Fe parameters being chosen as they are well studied in the literature and good parametrization exists from theory and experiments, providing a reasonable spin-phonon spectrum. For the sake of proof of concept, the system is effectively treated as an insulator—no electronic damping is considered on the spin system and the only thermostat is applied is acting on the lattice. The system size used in the simulations is $10 \times 10 \times 10$ bcc unit cells. For phonon interactions, we consider a Harmonic Potential (HP) and Morse Potential (MP). The HP is defined as $U(r_{ij}) = V_0(r_{ij} - r_{ij}^0)^2$, where V_0 has been parametrized for bcc Fe in Ref. [18] ($V_0 = 0.150$ eV/Å^2). The MP is defined as $U(r_{ij}) = D[e^{-2a(r_{ij}-r_0)} - 2e^{-a(r_{ij}-r_0)}]$ and is parameterized in Ref. [29] for bcc Fe ($D = 0.4174$ eV, $a = 1.3885$ Å, and $r_0 = 2.845$ Å). For both potentials, the interaction range was restricted to $r_c = 7.8$Å. The potentials we have chosen are fundamentally phenomenological, however, for the system and temperature range studied here, we have shown in Ref. [15] that several equilibrium spin wave-based properties, such as damping and equilibrium magnetization are not influenced by the choice of potential. Additionally, comparison with experimental phonon spectra shown in Ref. [15] showed good agreement for the Morse potential. Other works such as Ref. [19] include full first-principles parametrization of the mechanical potential and exchange interaction, so future work can benefit from such models.

The total Hamiltonian used in the simulations consists of the mechanical energy contributions [kinetic and potential energy $U(r_{ij})$] and the spin (magnetic) Hamiltonian—Eq. (1). The magnetic energy terms in our simulations [15] are the exchange interaction, uniaxial anisotropy with the easy axis $\mathbf{e}$ parallel to the z direction to mimic the switching experiments and a spin-lattice coupling Hamiltonian, given by the pseudodipolar coupling term ($\mathcal{H}_c$) [31,32], which we will describe later. The exchange interactions used in our simulations depend on atomic separation $J(r_{ij}) = J_0(1 - \frac{r_{ij}}{r_c})^3\Theta(r_c - r_{ij})$, where r_c is the cutoff and $\Theta(r_c - r_{ij})$ is the Heaviside step function. They were calculated from first-principles- methods for bcc Fe by Ma *et al.* [16]. The magnitude of the spin-lattice coupling is assumed to decay as $f(\mathbf{r}_{ij}) = CJ_0/r_{ij}^4$ as presented in Ref. [18] with C taken as a constant, for simplicity, measured relative to the exchange interactions J_0 ($CJ_0 = 0.452$ eV Å^4). The coupling strength C can be parameterized via the strain-dependent magnetoelastic anisotropy or via the value of the damping of the magnon (phonon) origin [15]. It is also possible to parametrize spin-lattice coupling terms as shown in Ref. [26] that accurately describe magnetoelastic phenomena, these methods being crucial for high-throughput computation development [33].

$$\begin{aligned}\mathcal{H}_{\text{tot}} = &\sum_i \frac{m_i \mathbf{v}_i^2}{2} + \frac{1}{2}\sum_{i,j} U(r_{ij}) - \frac{1}{2}\sum_{i,j} J(r_{ij})(\mathbf{S}_i \cdot \mathbf{S}_j) \\ &- \sum_i \mu_i (\mathbf{S}_i \cdot \mathbf{e})^2 \\ &- \sum_{i,j} f(r_{ij})\left[(\mathbf{S}_i \cdot \hat{\mathbf{r}}_{ij})(\mathbf{S}_j \cdot \hat{\mathbf{r}}_{ij}) - \frac{1}{3}\mathbf{S}_i \cdot \mathbf{S}_j\right], \end{aligned} \tag{1}$$

Since the total Hamiltonian depends on the coupled spin and lattice degrees of freedom ($\mathbf{v}_i$, $\mathbf{r}_i$, $\mathbf{S}_i$), the following equations of motion (EOM) need to be solved concurrently to obtain the dynamics of our coupled system:

$$\frac{\partial \mathbf{r}_i}{\partial t} = \mathbf{v}_i, \tag{2}$$

$$\frac{\partial \mathbf{v}_i}{\partial t} = -\eta \mathbf{v}_i + \frac{\mathbf{F}_i}{m_i}, \tag{3}$$

$$\frac{\partial \mathbf{S}_i}{\partial t} = -\gamma \mathbf{S}_i \times \mathbf{H}_i, \tag{4}$$

where $\mathbf{F}_i$ and $\mathbf{H}_i$ represent the effective force and field defined as $\mathbf{F}_i = -\frac{\partial \mathcal{H}_{tot}}{\partial \mathbf{r}_i} + \Gamma_i$ and $\mathbf{H}_i = -\frac{1}{\mu_S \mu_0}\frac{\partial \mathcal{H}_{\text{tot}}}{\partial \mathbf{S}_i}$. The term $\mathbf{\Gamma}_i$ represents the fluctuation term (thermal force) as expressed within Langevin dynamics and η represents the friction term that controls the dissipation of energy from the lattice into the external thermal reservoir. The thermal force has the form of a

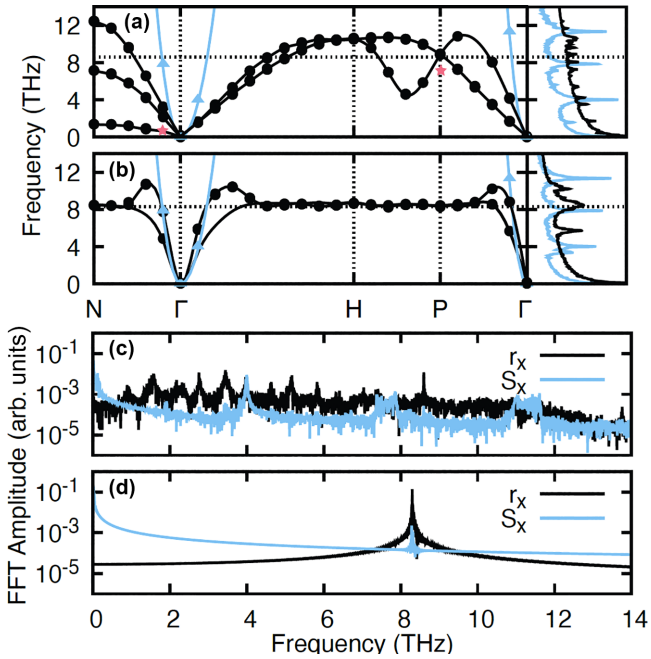

FIG. 2. Phonon (black points) and magnon (blue line points) spectra and density of states (right panel, continuous lines) of the x component of velocities and spins, respectively at T=10 K for a Morse potential [(a): MP] and Harmonic potential [(b): HP]. The continuous black lines in the left figure in (a) and (b) represent the spectra calculated using all three components of velocities. The red symbols in (a) show where we excite the system (close to Γ and in P point). The Fourier transform of spin (magnons) and position (phonons) after excitation with THz pulse for (c) MP at 8.6THz and (d) HP at 8.3THz. For completeness, we also show the Fourier transform of the magnons and phonons for a THz pulse for MP at 8.3THz and HP at 8.6THz in the Supplemental Material [30], Fig. S6.

Gaussian noise with the strength of the fluctuation term being expressed as $\frac{2\eta k_B T}{m_i}$.

For the spin degrees of freedom, we solve only the precessional Landau-Lifshitz equation: $\frac{\partial \mathbf{S}_i}{\partial t} = -\gamma \mathbf{S}_i \times \mathbf{H}_i$ without the Gilbert damping term, as this appears intrinsically in our model via the direct coupling to the lattice. However, later, to show the long-time scale behavior of the results, Fig. 4, we have employed a Landau-Lifshitz-Gilbert equation in the form: $\frac{\partial \mathbf{S}_i}{\partial t} = -\frac{\gamma}{(1+\lambda_G^2)} \mathbf{S}_i \times (\mathbf{H}_i + \lambda_G \mathbf{S}_i \times \mathbf{H}_i)$.

To model the effect of THz phonon excitation, we apply a periodic external force to each atom $F^{\alpha}_{\mathrm{THz}}(t, \mathbf{r}) = f^{\alpha}_0 \cos(2\pi \nu t + \mathbf{k} \cdot \mathbf{r}) \Theta(t_p - t)$, where $\Theta(t_p - t)$ is the Heaviside step function, t_p is the rectangular pulse duration, and α stands for the x, y, z coordinates of the forces. The excitation force F^{x}_{THz} is nonhomogeneous in space by choosing different k vectors and for simplicity is applied along the x direction.

III. THZ SWITCHING

The complete magnon-phonon spectrum is presented in Fig. 2. Note that for the HP, the phonon and magnon spectrum intersect, however, the MP does not present this feature. The power spectral density of the autocorrelation function in the frequency domain [15] (see also Fig. S1 in Supplemental Material) [30] reveals a peak for phonons at frequencies around 8.3 THz for the HP and a broad-band excitation for the MP around the similar frequency (with no available spin-wave modes), hence we first excite our systems around 8 THz. The application of the THz force drives the atom displacement to excite phonons within the system. Within the spin-lattice framework, these phonons break the local symmetry of the lattice which, through the pseudodipolar coupling term, generates an internal field capable of switching the magnetization. The k vector corresponding to the P point (obelisk symbol in Fig. 2) and the application of the force on the x direction was selected, as it gives rise to movement of the atoms entirely out of phase along the x direction, with oscillations of the atoms around their equilibrium position up to 7% of the lattice spacing (for $f^x_0 = 0.05$)—Supplemental Material, Fig. S4. In the case of the HP [Fig 2(b)], forced excitation with a THz pulse of 8.3 THz leads only to a response at the same frequency for both magnons (spin S_x) and phonons (position r_x) [Fig. 2(d)]. For the MP, although we excite the system only on the x direction and at the P point in the Brillouin zone, we observe multiple spin and phonon modes [Fig. 2(c)], reflecting the decay of the forced excitation into other modes, along the $P - \Gamma'$ path. This gives rise to displacements in all three directions, (Fig. S4, Supplemental Material) and a more complicated switching pattern and additional heating (as observed later in Figs. 3 and 6). Note that the analysis of the coupling fields (see Supplemental Material, Fig. S1) shows a broadening of the spectra at the excitation frequency for the MP, in contrast with the peak observed for the HP, suggesting a much weaker coupling to the THz force (hence a lower peak amplitude at the excitation frequency).

In spite of these differences in the excitation spectrum, we have observed magnetization switching for both potentials. Figure 3 shows examples of switching cases for HP [Fig. 3(a)] and MP [Fig. 3(c)]. The origin of the switching can be understood analyzing the behavior of the coupling fields which are responsible for magnetoelastic effects. We observe that the parallel to the magnetization component of the coupling field $H_c^{\parallel}$ is zero, and the THz excitation leads to the apparition of a perpendicular component $H_c^{\perp}$, which will drive the switching. In the case of the HP [Fig. 3(a)], we observe that at around 40 ps there is an increase in the $H_c^{\perp}$, leading to the initiation of switching. For the case shown in Fig. 3(b), the perpendicular field developed is smaller and cannot lead to switching. For MP, we observe that the perpendicular coupling field fluctuates due to the wider range of excited phonons. The switching is triggered when this field reaches a relatively constant, large value, which is a random event. For the case of Fig. 3(d), no switching is triggered since the in-plane component of the perpendicular field is rotating (see Fig. S5 in Supplemental Material). Importantly, after the THz excitation, the magnetoelastic fields are almost zero, showing that all the energy was transferred and used during the switching. After this time, the only effective field that leads the magnetic system back to saturation is a small uniaxial anisotropy, $H_a^z = 0.05$T, which defines a slow relaxation of the system at much longer timescales (>30 ns) than those presented here. We conclude that the reason for magnetization switching is the generation

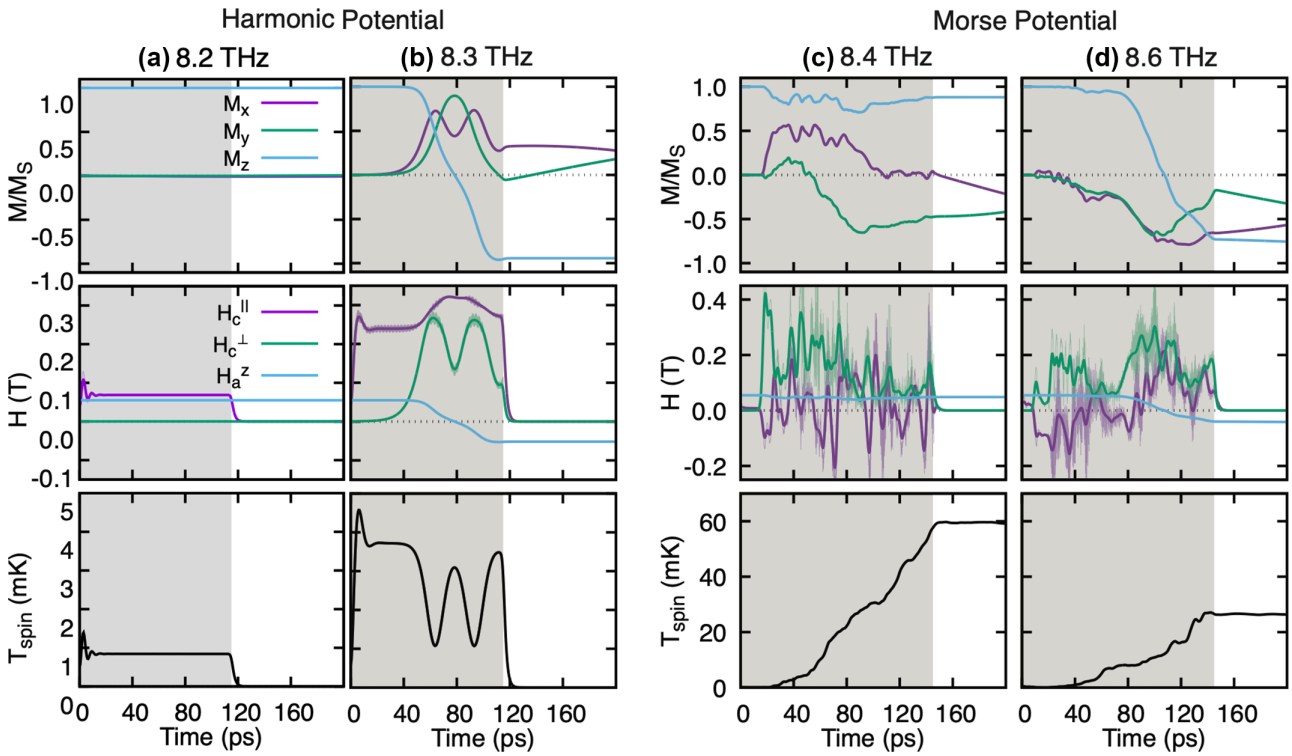

FIG. 3. Evolution of magnetization (top row), coupling and anisotropy fields (middle row), and spin temperature (bottom row) under the application of a THz pulse for the Harmonic [(a), (b)] and Morse potential [(c), (d)]. For each potential, two frequencies are shown; one where switching does not occur [(a), (b)] and where switching did occur [(b), (d)]. The temporal region where the THz pulse is applied is emphasized by the gray area; which for (a) and (b) is 115 ps and for (c) and (d) is 145 ps.

of sufficiently strong perpendicular to magnetization fields of of magnetoelastic origin.

IV. EXTENDED TIMESCALE RESULTS

To characterize the spin system, we calculate the spin temperature [34]; see Fig. 3, bottom panels. We observe that the increase of temperature is in the mK range, proving the lack of heating during this process. Moreover, the spin temperature in the case of the HP is raised to several mK while approximately 10 times larger temperatures (around 10 mK and up to 28 mK) are created for the MP. In the case of the HP, the very small temperature increase is due to the fact that no magnons can be excited in the spin system and thus the energy goes efficiently into the magnetoelastic fields created by the spin-phonon coupling with the rest of the increase in temperature coming from switching only, as shown in Fig. S3, Supplemental Material. This underlines the main differences between the HP and anharmonic MP. In the latter case, large nonlinearities are present in the system. Since our excitations are strong, these nonlinearities act as an efficient scattering mechanism for phonons, which finally add a temperaturelike effect.

Figures 4 and 5 highlight the extended timescales observed in our simulations following the application of the THz pulse. When the magnetic system does not contain any electronic damping, the relaxation happens via the lattice only, which for low temperature is a very slow process. Consequently, during the timeframe depicted in Fig. 3(b), the magnetization appears to remain constant after the laser pulse application. Introducing an additional Gilbert damping λ_G after the application of the THz pulse as shown in the Fig. 4(a), we observe that the magnetization decays towards its equilibrium value, which in this case is (0,0,−1) in ns timescales. A slow dynamics can also be observed for the spin temperature in Fig. 3(c). After the THz pulse is stopped, the energy deposited in the system will slowly be washed out by the thermostat but at large timescales (about 6 mK/ns) as shown in Fig. 5. It's important to note that the slow relaxation is particular to the Morse potential, owing to its nonlinearities and the excitation of numerous spin-phonon modes during the THz pulse.

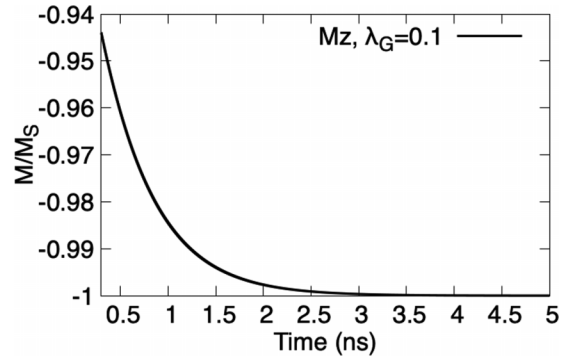

FIG. 4. Evolution of the z component of magnetization (M_z) for up to 5 ns when the Gilbert spin damping λ_G is turned on. The results are for a harmonic potential (HP), and the applied THz pulse properties are 8.3 THz and 115 ps.

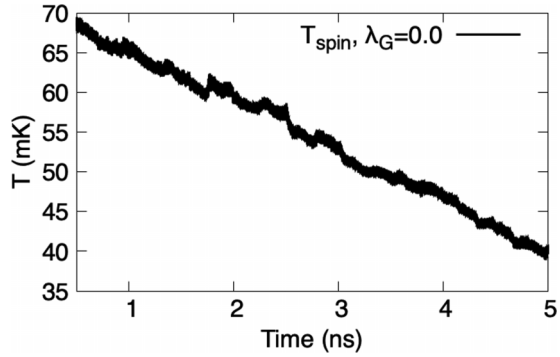

FIG. 5. Evolution of the spin temperature for up to 5 ns (bottom panel) in the case of Morse potential (MP). The applied THz pulse properties are 8.4 THz and 145 ps.

V. SWITCHING PHASE DIAGRAM AND ANGULAR MOMENTUM TRANSFER

Figure 6 shows the phase diagram for magnetization switching at $T = 0\,\mathrm{K}$ for HP (a) and MP (b) in terms of the excitation frequency and the pulse duration. An important difference between the two potentials is a much larger switching region for the MP, however, with scattered points due to phonon modes generation and finite-size (finite-time) effects which we will discuss below. We note that the excitation at this frequency produces a large phonon response, up to 5–7% of the interatomic distance (see Supplemental Material, Fig. S4) and many phonon modes are available at these frequencies. We underline that magnons do not have modes at these frequencies and the corresponding k point, hence the switching is triggered by phonons. During the switching, the change in the magnetization length is less than 0.04%, suggesting once more a nonthermal switching. Figures 6(c) and 6(d) show the final magnetization state for different pulse widths (points) after the application of a THz laser pulse. For longer pulse widths, there is an oscillatory behavior of the magnetization

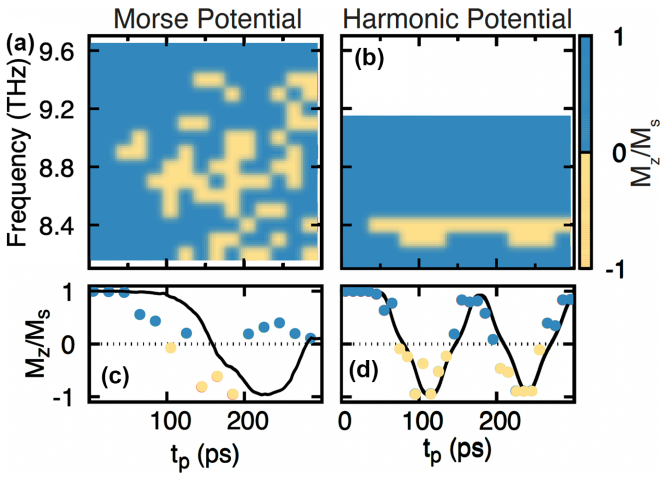

FIG. 6. Switching phase diagrams, $T = 0\,\mathrm{K}$ as a function of THz pulse frequency and duration of the pulse, Morse [MP: (a)] and Harmonic [HP: (b)] potential. (c), (d) Final magnetization after each THz pulse (points) and the magnetization during 295 ps pulse (continuous line).

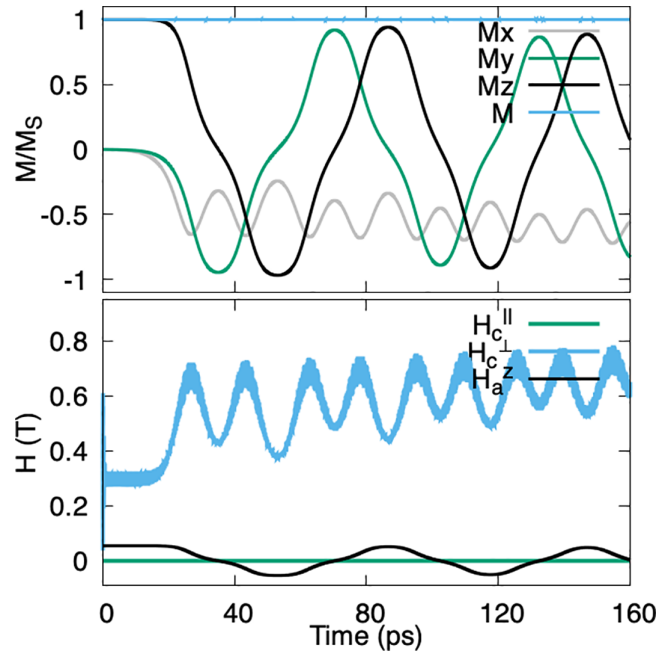

FIG. 7. Evolution of magnetization (M/M_S), coupling fields parallel and perpendicular to the direction of magnetization ($H_c^{\parallel}$ and $H_c^{\perp}$), anisotropy field (H_a^z) for an imposed harmonic variation of the x displacement of the atoms with a frequency of 8.4 THz.

which corroborates the precessional and coherent nature of the switching. The fluctuation of the in-plane coupling field for MP is responsible for random switching events visible in the phase diagram of Fig. 6, in contrast to the regular behavior of HP. The random switching effects are especially visible in small systems, as is the case of our simulations. Analyzing Figs. 6(c) and 6(d), we confirm that in the case of the MP [Fig. 6(c)], the scattering of the phonon modes and subsequent heating leads to a scattered final magnetic state with each realisation, while for the HP, a similar magnetic state is obtained with each realization. A similar randomization is produced when we analyze the switching diagrams at nonzero temperatures for the HP; see Supplemental Material, Fig. S2. This random switching diagram has also been reported for a macrospin nanoparticle with a magnetoelastic anisotropy term at nonzero temperature [12].

One of the main characteristics of the switching is that a minimum duration of the THz pulse around 50 ps is required, as shown by the phase diagram. A detailed examination shows that the switching is precessional due to the fact that the application of the force on the x direction for the k vector corresponding to the P point in the Brillouin zone generates a coupling field that acts in plane on the x direction (see Fig. 3). Additional proof is shown in Fig. 7, where we artificially impose an x displacement on atoms of the same magnitude, frequency, and phase as in the case of the direct numerical simulations with a HP. This periodic motion creates a perpendicular coupling field to the magnetization and leads to precessional switching.

To gain better understanding of the switching in terms of the angular momentum transfer, we have computed the phonon angular momentum defined as $\mathbf{L} = \sum(\mathbf{r}_i \times m_i \mathbf{v}_i)$ and

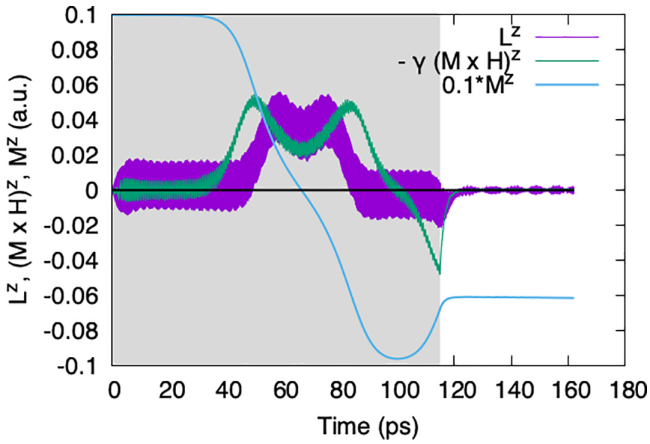

FIG. 8. Evolution of the z component of angular momentum, L^z, magnetization (M^z), and magnetic torque $\gamma(\mathbf{M} \times \mathbf{H})^z$ for the THz switching with a Harmonic potential at a frequency of 8.3 THz and a pulse width of 115 ps.

magnetic torque during a switching event—Fig. 8. During the period in which the system is excited by the THz pulse (highlighted in gray), there is a a minimal phonon angular momentum (L^z). This arises from atomic-level spin precession, driven by the in-plane pseudodipolar field, resulting in angular momentum within the phonon system. However, this transfer of angular momentum alone is insufficient to account for switching, as it necessitates significantly larger magnitudes. Moreover, all the angular momentum generated during the switching dissipates back to the lattice, and we can clearly observe that after we stop pumping, since the phonon angular momentum decreases to zero.

VI. NEAR Γ-POINT THz EXCITATION

Finally, Fig. 9 presents the results of lower frequency THz-phonon excitation near the Γ point (at the red asterix symbol in Fig. 2) for the MP and for two excitation strengths. This is a characteristic example of what typically occurs in both systems. A small excitation, $f_0^x = 0.02$, does not develop any transverse coupling field and produces no effect except small-amplitude spin waves. Large excitation (for $f_0^x = 0.03$, average $H_c^t = 1.5$T) efficiently excites the spin system in a random way, leading to a large increase of its temperature. Hence, although excitation close to the Γ point produces random noncoherent switching events, for some particular excitation strengths, the process is associated with subsequent heating. The final spin temperature increases when the excitation strength increases.

VII. CONCLUSIONS

Using a spin-phonon model that allows for angular momentum transfer, we investigated the effect of magnetization switching driven by phonon excitations with minimal energy dissipation. SLD models are crucial for the investigation of magnetization switching via THz phonons, as we are able to access the magnetization dynamics corresponding to the excitation of individual or collective phonon modes. Our results suggest that ferromagnetic materials that present a flat phonon

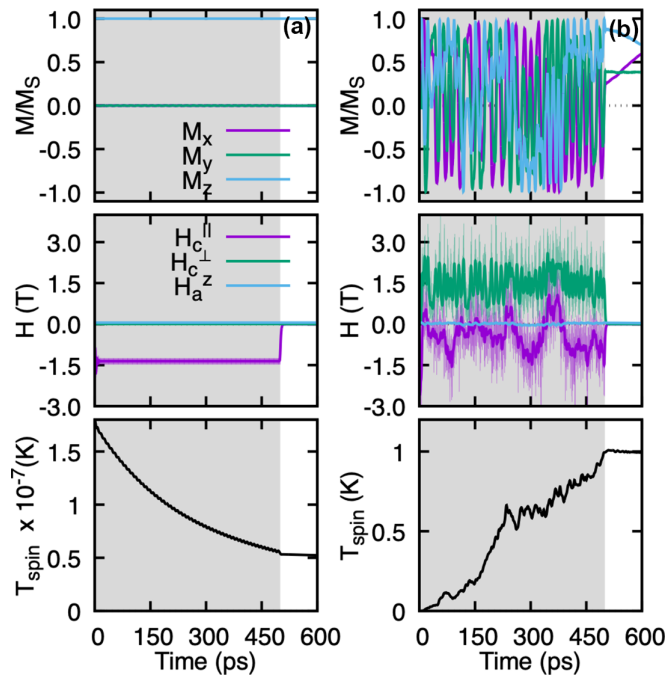

FIG. 9. Example of dynamics excited near Γ point at 0.4 THz for Morse potential and two excitation strengths: $f_0^x = 0.02$ (left) and $f_0^x = 0.03$ (right).

spectral region where a large number of phonon modes can be efficiently excited are good candidates for THz-assisted cold switching. The key factor is excitation with THz phonons with frequencies and k points at a maximum in the phonon density of states and no spin excitations. The mechanism corresponds to the phonon-driven generation of magnetoelastic fields with components perpendicular to the magnetization producing precessional switching on the 100 ps timescale. Importantly, we predict this possibility for the case of single species materials unlike early experimental observations [14] where the switching was due to optical phonon excitation. In this regard, the important factor is related to the possibility of experimental access to the excitation with k vectors close to this flat phonon spectrum; in our case, the P point. Our prediction may be of crucial importance for the next generation of ecofriendly storage devices, since heat production is one of the major problems for large data storage centers.

ACKNOWLEDGMENTS

Financial support of the Advanced Storage Research Consortium and ARCHER2-eCSE06-6 is gratefully acknowledged. M.O.A.E. gratefully acknowledges support in part from EPSRC through Grant No. EP/S009647/1. The simulations were undertaken on the VIKING cluster at the University of York. S.R., R.W.C., and R.F.L.E. acknowledge funding from European Union's Horizon 2020 Research and Innovation Program under Grant Agreement No. 737709. The authors acknowledge the networking opportunities provided by the European COST Action No. CA17123 Magnetofon and the short-time scientific mission awarded to M.S.

[1] E. Y. Vedmedenko, R. K. Kawakami, D. D Sheka, P. Gambardella, A. Kirilyuk, A. Hirohata, C. Binek, O. Chubykalo-Fesenko, S. Sanvito, B. J. Kirby *et al.*, The 2020 magnetism roadmap, J. Phys. D **53**, 453001 (2020).

[2] C. D. Stanciu, F. Hansteen, A. V. Kimel, A. Kirilyuk, A. Tsukamoto, A. Itoh, and Th. Rasing, All-optical magnetic recording with circularly polarized light, Phys. Rev. Lett. **99**, 047601 (2007).

[3] I. Radu, C. Stamm, A. Eschenlohr, F. Radu, R. Abrudan, K. Vahaplar, T. Kachel, N. Pontius, R. Mitzner, K. Holldack, A. Föhlisch, T. A. Ostler, J. H. Mentink, R. F. L. Evans, R. W. Chantrell, A. Tsukamoto, A. Itoh, A. Kirilyuk, A. V. Kimel, and Th. Rasing, Ultrafast and distinct spin dynamics in magnetic alloys, SPIN **05**, 1550004 (2015).

[4] T. Kampfrath, A. Sell, G. Klatt, A. Pashkin, S. Mährlein, T. Dekorsy, M. Wolf, M. Fiebig, A. Leitenstorfer, and R. Huber, Coherent terahertz control of antiferromagnetic spin waves, Nat. Photon. **5**, 31 (2011).

[5] C. Dornes, Y. Acremann, M. Savoini, M. Kubli, M. J. Neugebauer, E. Abreu, L. Huber, G. Lantz, C. A. F. Vaz, H. Lemke, E. M. Bothschafter, M. Porer, V. Esposito, L. Rettig, M. Buzzi, A. Alberca, Y. W. Windsor, P. Beaud, U. Staub, D. Zhu *et al.*, The ultrafast Einstein-de Haas effect, Nature (London) **565**, 209 (2019).

[6] D. Beaujouan, P. Thibaudeau, and C. Barreteau, Anisotropic magnetic molecular dynamics of cobalt nanowires, Phys. Rev. B **86**, 174409 (2012).

[7] S. F. Maehrlein, I. Radu, P. Maldonado, A. Paarmann, M. Gensch, A. M. Kalashnikova, R. V. Pisarev, M. Wolf, P. M. Oppeneer, J. Barker *et al.*, Dissecting spin-phonon equilibration in ferrimagnetic insulators by ultrafast lattice excitation, Sci. Adv. **4**, eaar5164 (2018).

[8] A. Melnikov, I. Radu, U. Bovensiepen, O. Krupin, K. Starke, E. Matthias, and M. Wolf, Coherent optical phonons and parametrically coupled magnons induced by femtosecond laser excitation of the Gd(0001) Surface, Phys. Rev. Lett. **91**, 227403 (2003).

[9] D. Afanasiev, J. R. Hortensius, B. A. Ivanov, A. Sasani, E. Bousquet, Y. M. Blanter, R. V. Mikhaylovskiy, A. V. Kimel, and A. D. Caviglia, Ultrafast control of magnetic interactions via light-driven phonons, Nat. Mater. **20**, 607 (2021).

[10] D. Afanasiev, I. Razdolski, K. M. Skibinsky, D. Bolotin, S. V. Yagupov, M. B. Strugatsky, A. Kirilyuk, Th. Rasing, and A. V. Kimel, Laser excitation of lattice-driven anharmonic magnetization dynamics in dielectric $FeBO_3$, Phys. Rev. Lett. **112**, 147403 (2014).

[11] R. M. Otxoa, U. Atxitia, P. E. Roy, and O. Chubykalo-Fesenko, Giant localised spin-Peltier effect due to ultrafast domain wall motion in antiferromagnetic metals, Commun. Phys. **3**, 31 (2020).

[12] V. S. Vlasov, A. M. Lomonosov, A. V. Golov, L. N. Kotov, V. Besse, A. Alekhin, D. A. Kuzmin, I. V. Bychkov, and V. V. Temnov, Magnetization switching in bistable nanomagnets by picosecond pulses of surface acoustic waves, Phys. Rev. B **101**, 024425 (2020).

[13] O. Kovalenko, T. Pezeril, and V. V. Temnov, New concept for magnetization switching by ultrafast acoustic pulses, Phys. Rev. Lett. **110**, 266602 (2013).

[14] A. Stupakiewicz, C. S. Davies, K. Szerenos, D. Afanasiev, K. S. Rabinovich, A. V. Boris, A. Caviglia, A. V. Kimel, and A. Kirilyuk, Ultrafast phononic switching of magnetization, Nat. Phys. **17**, 489 (2021).

[15] M. Strungaru, M. O. A. Ellis, S. Ruta, O. Chubykalo-Fesenko, R. F. L. Evans, and R. W. Chantrell, Spin-lattice dynamics model with angular momentum transfer for canonical and microcanonical ensembles, Phys. Rev. B **103**, 024429 (2021).

[16] P.-W. Ma, C. H. Woo, and S. L. Dudarev, Large-scale simulation of the spin-lattice dynamics in ferromagnetic iron, Phys. Rev. B **78**, 024434 (2008).

[17] D. Perera, M. Eisenbach, D. M. Nicholson, G. M. Stocks, and D. P. Landau, Reinventing atomistic magnetic simulations with spin-orbit coupling, Phys. Rev. B **93**, 060402 (2016).

[18] M. Aßmann and U. Nowak, Spin-lattice relaxation beyond Gilbert damping, J. Magn. Magn. Mater. **469**, 217 (2019).

[19] J. Hellsvik, D. Thonig, K. Modin, D. Iuşan, A. Bergman, O. Eriksson, L. Bergqvist, and A. Delin, General method for atomistic spin-lattice dynamics with first-principles accuracy, Phys. Rev. B **99**, 104302 (2019).

[20] J. Tranchida, S. J. Plimpton, P. Thibaudeau, and A. P. Thompson, Massively parallel symplectic algorithm for coupled magnetic spin dynamics and molecular dynamics, J. Comput. Phys. **372**, 406 (2018).

[21] J. R. Cooke III and J. R. Lukes, An implicit spin lattice dynamics integrator in LAMMPS, Comput. Phys. Commun. **271**, 108203 (2022).

[22] W. Dednam, C. Sabater, A. E. Botha, E. B Lombardi, J. Fernández-Rossier, and M. J. Caturla, Spin-lattice dynamics simulation of the Einstein–de Haas effect, Comput. Mater. Sci. **209**, 111359 (2022).

[23] J. R. Cooke and J. R. Lukes, Angular momentum conservation in spin-lattice dynamics simulations, Phys. Rev. B **107**, 024419 (2023).

[24] G. Dos Santos, R. Meyer, D. Tramontina, E. M. Bringa, and H. M. Urbassek, Spin-lattice-dynamics analysis of magnetic properties of iron under compression, Sci. Rep. **13**, 14282 (2023).

[25] M. Weißenhofer, H. Lange, A. Kamra, S. Mankovsky, S. Polesya, H. Ebert, and U. Nowak, Rotationally invariant formulation of spin-lattice coupling in multiscale modeling, Phys. Rev. B **108**, L060404 (2023).

[26] P. Nieves, J. Tranchida, S. Arapan, and D. Legut, Spin-lattice model for cubic crystals, Phys. Rev. B **103**, 094437 (2021).

[27] S. Mankovsky, S. Polesya, H. Lange, M. Weißenhofer, U. Nowak, and H. Ebert, Angular momentum transfer via relativistic spin-lattice coupling from first principles, Phys. Rev. Lett. **129**, 067202 (2022).

[28] S. Nikolov, M. A. Wood, A. Cangi, J.-B. Maillet, M.-C. Marinica, A. P. Thompson, M. P. Desjarlais, and J. Tranchida, Data-driven magneto-elastic predictions with scalable classical spin-lattice dynamics, npj Comput. Mater. **7**, 153 (2021).

[29] L. A. Girifalco and V. G. Weizer, Application of the morse potential function to cubic metals, Phys. Rev. **114**, 687 (1959).

[30] See Supplemental Material at http://link.aps.org/supplemental/10.1103/PhysRevB.109.224412 for complementary results on different switching scenarios (such as finite temperature

switching, switching in a constant field) or additional plots of displacements and power spectral density.

[31] A. I. Akhiezer, S. V. Peletminskii, and V. G. Baryakhtar, *Spin Waves* (North-Holland, Amsterdam, 1968).

[32] S. Chikazumi and C. D. Graham, *Physics of Ferromagnetism* (Oxford University Press, Oxford, 1997), Vol. 94.

[33] P. Nieves, S. Arapan, S. H. Zhang, A. P. Kądzielawa, R. F. Zhang, and D. Legut, Automated calculations of exchange magnetostriction, Comput. Mater. Sci. **224**, 112158 (2023).

[34] P.-W. Ma, S. L. Dudarev, A. A. Semenov, and C. H. Woo, Temperature for a dynamic spin ensemble, Phys. Rev. E **82**, 031111 (2010).